Smart Mater. Struct. **18** (2009) 085023 (9pp) doi:10.1088/0964-1726/18/8/085023

An autonomous battery-less sensor module powered by piezoelectric energy harvesting with RF transmission of multiple measurement signals

Marco Ferrari, Vittorio Ferrari, Michele Guizzetti and Daniele Marioli

Department of Electronics for Automation, University of Brescia, Via Branze 38, I-25123 Brescia, Italy

E-mail: vittorio.ferrari@ing.unibs.it

Received 12 December 2008, in final form 14 May 2009
Published 23 July 2009
Online at stacks.iop.org/SMS/18/085023

Abstract

An energy-autonomous battery-less sensor module is presented, entirely powered by a piezoelectric energy converter driven by mechanical vibrations from the environment. The module manages and stores the converted energy, interfaces to one or more passive sensors and periodically sends the corresponding measurement signals over a radio-frequency (RF) link. As an additional variant, the module can send a programmable identification (ID) code on the RF carrier, in order to enable module tagging and tracking by the external receiver unit. The module's general architecture is presented and the strategy used for sensor signal conditioning and transmission is illustrated. The architecture and principle have been experimentally validated on a fabricated prototype including a piezoelectric bimorph converter, two passive sensors made by a resistive–capacitive sensor pair and purposely designed electronic circuitry based on low-power off-the-shelf components. In the tested experimental conditions, the prototype features a typical time interval between measurement-and-transmission events of a few tens of seconds, with event durations of the order of tens of milliseconds, corresponding to an operation duty cycle of the order of 0.1%. Peak power consumption during transmission is of the order of 20 mW and operative range is of the order of meters in a laboratory environment. The obtained results show that the proposed approach has attractive characteristics because of the total absence of batteries and, despite the inherent intermittent operation, provides significant measurement performances in terms of achievable sensitivity and resolution.

(Some figures in this article are in colour only in the electronic version)

1. Introduction

In the fields of instrumentation, measurement and monitoring systems, the topic of power harvesting is increasingly considered a key point in the development of autonomous sensing nodes and microsystems with extended lifetimes in unattended operation [1–5]. Among the power harvesting methods, the conversion of mechanical energy from background vibrations into electrical energy via the piezoelectric effect is particularly effective, due to the ubiquitous presence of vibrations and the availability of piezoelectric materials of adequate performance [6–13].

A general problem with power harvesting units, in particular for the case of vibration-driven converters, is that the output power is often too low and/or discontinuous to guarantee a continuous operation of the electric load represented by the system at hand. To overcome this limitation, a rechargeable battery can be present to power the system, while the harvested energy is used for trickle charging of the battery to extend its lifetime. On-board energy sources are also used to supply optimized power management circuits [14, 15].

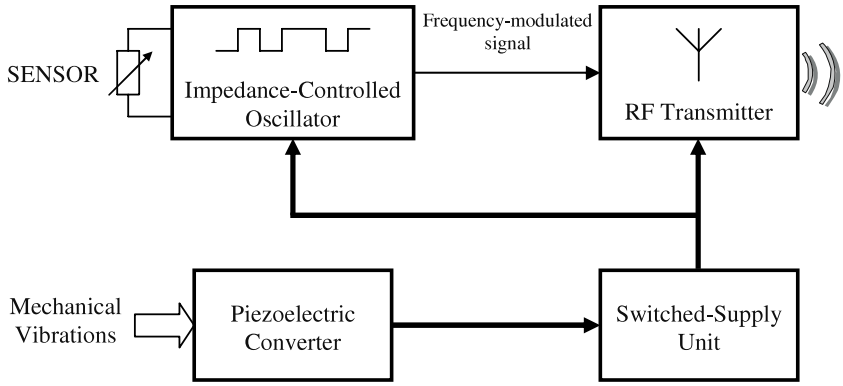

Figure 1. Block diagram of the proposed architecture for a vibration-powered autonomous sensor module with RF measurement signal transmission.

As a more appealing solution because it is entirely battery-less, the converted energy can be accumulated by proper power management techniques and then transferred to the load during time intervals of relatively short duration, thereby granting suitable power, albeit for a limited time. This unavoidably causes a switched supply of the system which results in intermittent operation. With sensors and measuring systems as the load, the intermittent operation poses new challenges to develop techniques and strategies that meet the demand for suitable metrological performances under the combined constraints of low-power consumption and switched-supply functioning.

In this context, an energy-autonomous battery-less sensor module, entirely powered by a piezoelectric energy converter, is here presented. The converted electrical energy is stored and used for the intermittent ignition of a low-power radio-frequency (RF) transmitter capable of periodically transferring over a short-range link the information coming from one or more sensors.

The general architecture of the module is presented, and the strategy used for sensor signal conditioning and transmission is illustrated. Prototypes of the module have been built and tested. The obtained experimental results demonstrate the possibility of using the module to power two passive variable-impedance sensors, e.g. resistive and/or capacitive sensors, and periodically transmit their readings via the frequency modulation of the envelope of the RF carrier. As an addition, the module has been equipped with the provision of a programmable identification (ID) code also sent on the signal RF carrier, in order to enable module tagging and tracking.

2. Proposed approach

Piezoelectric converters of suitably low size operated by vibrations can supply electrical power ranging from hundreds of nanowatts to a few milliwatts at mechanical resonance [1, 6]. The associated energy can be accumulated and used in purposely designed low-power battery-less microsystems working in switched-supply mode.

Due to the power budget, intermittent operation with a very low duty cycle is mandatory, while component count and circuit complexity must be kept to a minimum. With such constraints, adequate techniques must be adopted for sensor signal conditioning to ensure the required resolution and accuracy.

The general block diagram of the sensor module is shown in figure 1, which exemplifies the architecture. In the proposed approach, a passive sensor, i.e. a modulating sensor such as a variable-impedance device, is inserted as the frequency-determining element of a low-power relaxation oscillator, which in turn is used for on–off keying (OOK) frequency modulation of the envelope of the transmitted RF carrier [16, 17]. Both the oscillator and the RF transmitter are powered by the piezoelectric harvester via the switched-supply unit, which manages the converted energy and periodically delivers it to the load, thereby causing intermittent operation.

By means of frequency modulation, measurement information is sent as an analog quantity on the timescale and, due to the ratiometric operation of relaxation oscillators, it has the advantage that is not affected by reference voltage levels in the circuit that are intrinsically poorly defined due to transient operation.

In the present work the architecture illustrated in figure 1 has been modified to be extended to more than one sensor. In particular, figure 2 shows the block diagram of the autonomous sensor module that has been developed to interface with two sensors and send their respective measurement signals.

The electrical power coming from the converter is rectified and the energy is stored in the capacitor C_b. An ultra-low-loss sensing-and-switching circuit based on MOS transistors controls the energy transfer from the storage capacitor C_b to the load by managing the cyclic evolution of the capacitor voltage between two preset threshold levels, therefore realizing a switched-supply unit. When the voltage V_C on the capacitor C_b reaches the high threshold level, the stored energy is transferred to a voltage regulator and, in cascade, to a power-switching stage to sequentially supply two separate sensor oscillators and to a low-power RF transmitter driven by the sensor oscillator outputs. The power-switching stage is formed by a monostable circuit controlling a single-pole double-throw (SPDT) active switch. Therefore, the transmitted RF burst upon discharge of C_b is composed by a sequence of two frames. The first and second frames have the frequency respectively determined by

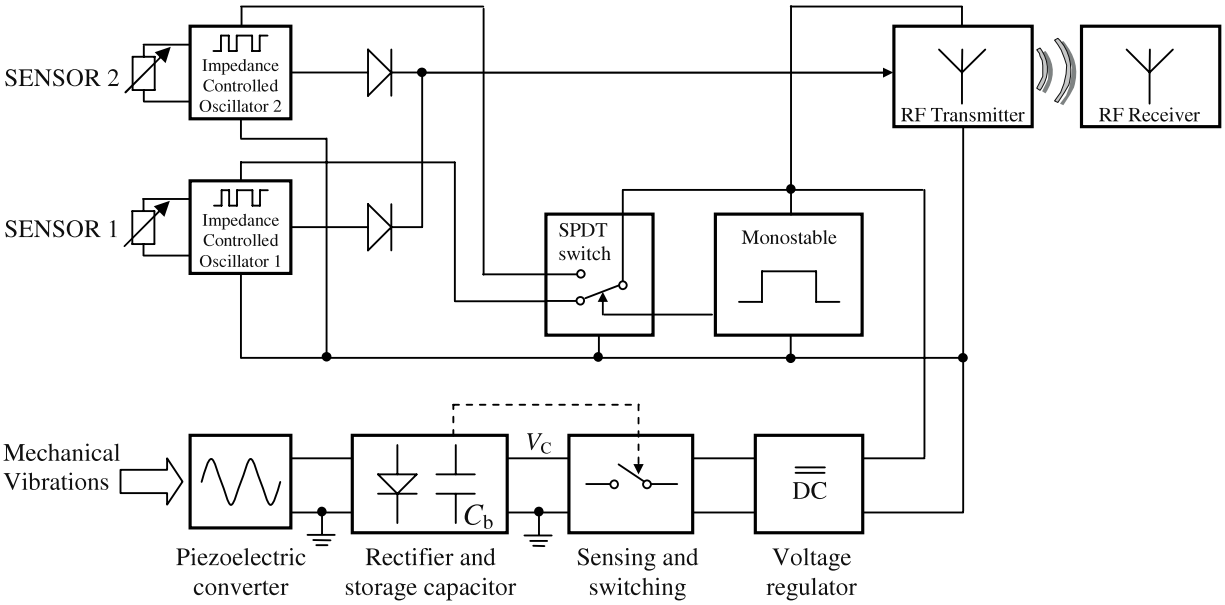

Figure 2. Block diagram of the developed autonomous sensor module.

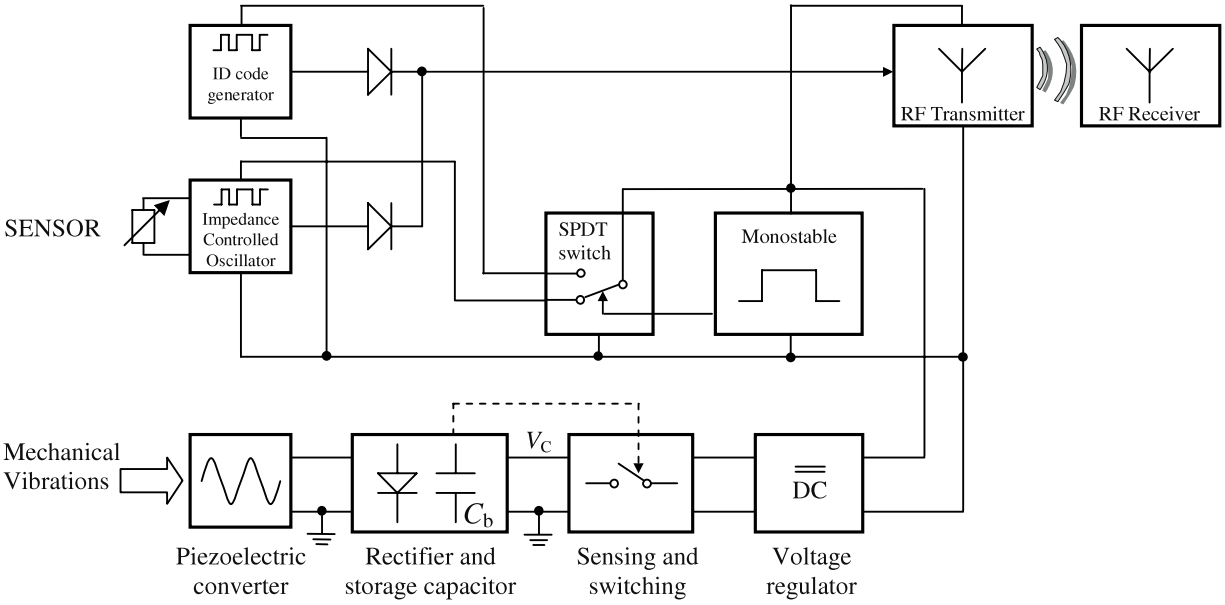

Figure 3. Block diagram of the developed autonomous sensor module with ID code transmission.

sensor 1 and sensor 2. When V_C reaches the low threshold level, the sensing-and-switching circuit disconnects the load and the charge cycle of C_b restarts.

An additional proposed version of the autonomous sensor module is shown in figure 3, in which sensor 2 is replaced by an ID code generation circuit. In this way the first frame of the RF burst carries the measurement information of the sensor, while the second frame contains the ID code as a tag of the transmitting sensor unit. When multiple autonomous sensor modules are located in the same area, the ID code enables the external receiver to unequivocally identify and track the source of the transmitted measurement information.

3. Autonomous sensor module

A prototype of the autonomous sensor module, following the architecture of figure 2, was breadboarded using off-the-shelf components as shown in the circuit diagram of figure 4.

Piezoelectric harvesters can be manufactured in different technologies and geometries [16, 18, 19]. We have focused on converters based on simple flexure elements with the shape of cantilever beams. An example of a converter based on PZT thick films that was first tested to power the autonomous sensor module is shown in figure 5(a) [16]. To reduce size, a different piezoelectric element was used as the converter

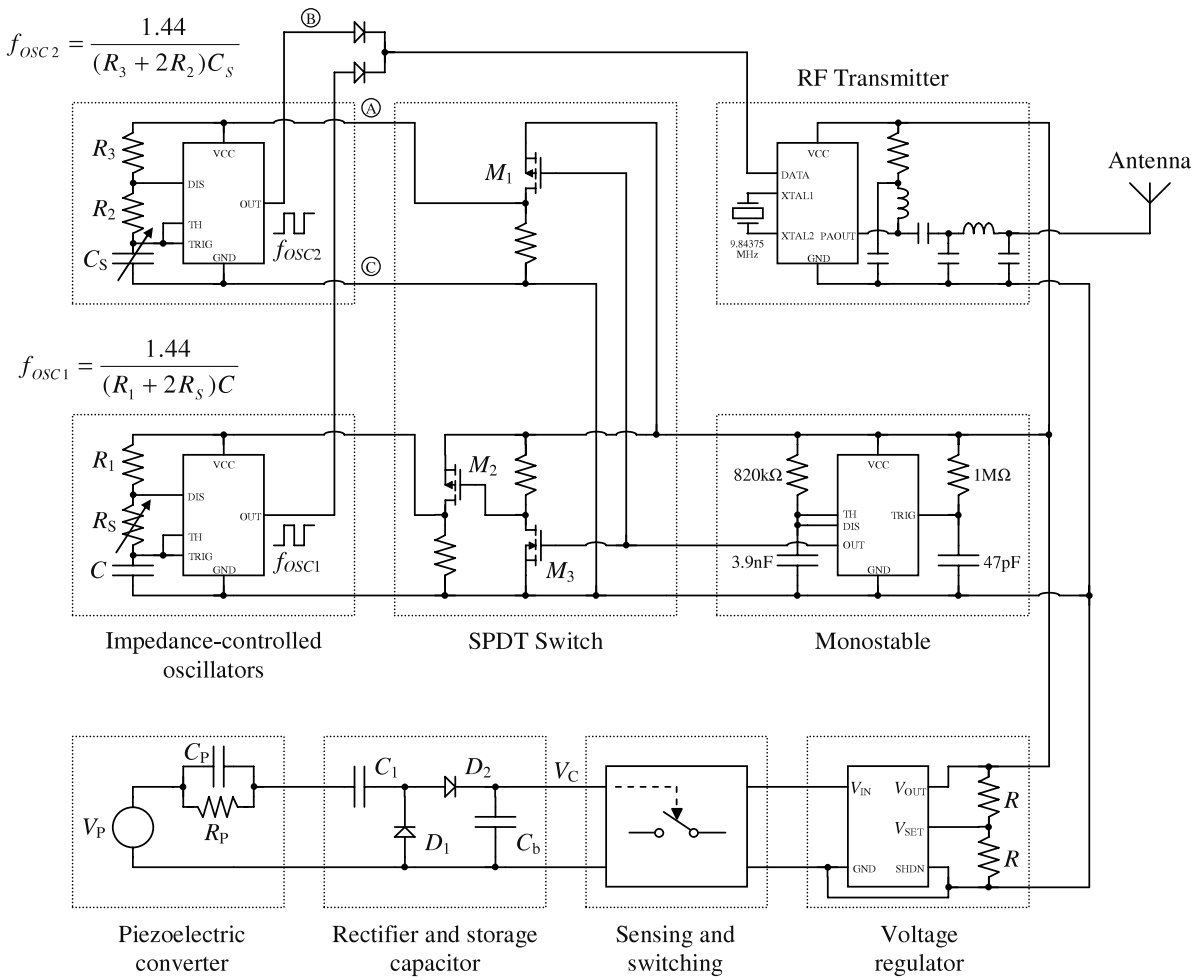

Figure 4. Electrical diagram of the developed autonomous sensor module.

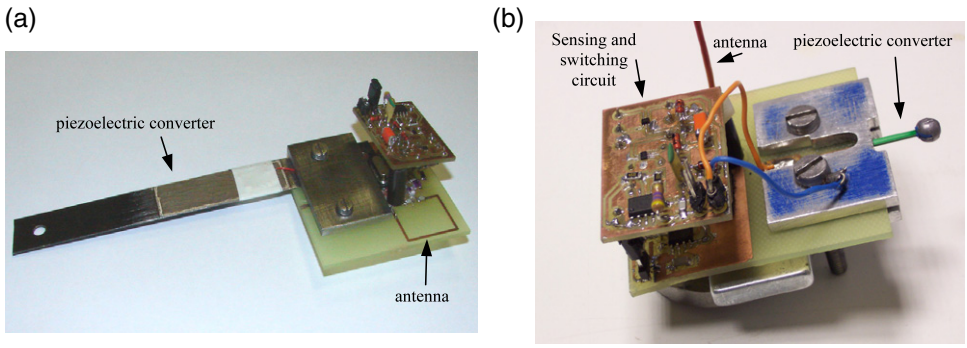

Figure 5. The realized prototype of the autonomous sensor module with a thick-film piezoelectric converter (a) and with a commercial piezoelectric converter (b).

in this study. It is a commercial piezoelectric bimorph, (RS Components, code 285–784), with dimensions of (15 × 1.5 × 0.6) mm^3. As shown in figure 5(b), a mass was attached to the cantilever tip, thereby setting the mechanical resonant frequency at a value to be around 250 Hz. In figure 4 the piezoelectric converter is represented by its low-frequency Thevenin equivalent circuit [16]. In the model, V_P represents the frequency-dependent open-circuit voltage, which nulls for $\omega = 0$, and R_P and C_P represent the equivalent resistance and capacitance, respectively. R_P and C_P have been measured with an impedance analyzer (HP4194A) at a frequency of around 250 Hz, obtaining values of 40 MΩ and 840 pF, respectively.

The output voltage of the piezoelectric converter is rectified by means of the circuit made by C_1, D_1, D_2 and C_b. Diodes D_1 and D_2 are of 1N4148 type that ensure low reverse leakage currents.

Assuming the voltage V_P to be sinusoidal with period T, at each period a discrete amount of charge is transferred from the piezoelectric converter to the storage capacitor C_b.

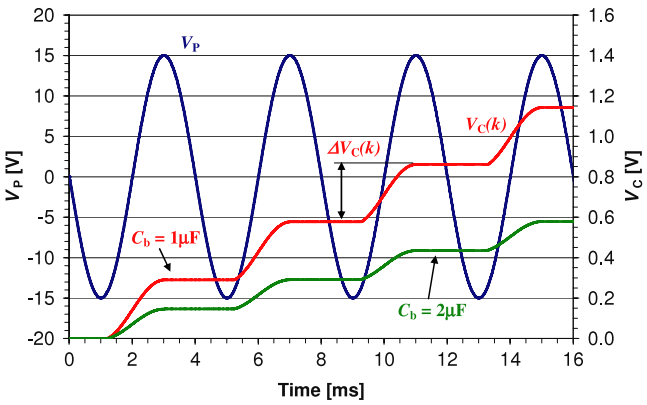

Figure 6. PSpice simulation results of the rectifier and storage circuit for different values of C_b ($V_{PM} = 15$ V; $C_{P1} = 10$ nF).

Therefore, the voltage V_C across the storage capacitor increases with stepwise behavior described by the sequence $V_C(k)$ where k is the index of the period considered.

Neglecting the resistor R_P due to its high value, assuming ideal diodes, and indicating with C_{P1} the series combination of C_P and C_1, the kth voltage increment $\Delta V_C(k)$ can be expressed as [20]:

$$\Delta V_C(k) = \frac{C_{P1}}{C_{P1} + C_b} (2V_{PM} - V_C(k-1)) \qquad (1)$$

where V_{PM} is the peak amplitude of the voltage V_P.

In practice, the capacitance C_{P1} is dominated by C_P resulting in $C_{P1} \approx C_P$ and C_1 is not strictly required. To maximize the voltage increments $\Delta V_C(k)$ and shorten the charging cycle, it should be $C_P \gg C_b$. But, considering the typical values of C_P, this would imply a value of C_b impractically low to store enough energy at voltages V_C of the order of a few volts. As a consequence, C_b has to be chosen so that $C_b \gg C_{P1} \approx C_P$ and in equation (1) it holds that $C_{P1}/(C_{P1} + C_b) \approx C_P/(C_P + C_b) \ll 1$.

Expliciting the voltage $V_C(k)$ across the storage capacitor as a function of the period index k the following expression can be obtained:

$$V_C(k) = 2V_{PM}\left[1 - \left(\frac{C_b}{C_P + C_b}\right)^k\right]. \qquad (2)$$

Equation (2) shows that $V_C(k)$ has an exponential envelope asymptotically reaching a steady-state value of $2V_{PM}$, resulting in a voltage doubler behavior.

Figure 6 shows typical PSpice simulation results, plotting the voltage V_P generated by the piezoelectric converter and the voltage $V_C(k)$ across the storage capacitor for different values of C_b. The stepwise behavior of $V_C(k)$ can be clearly seen.

Considering the charge of the storage capacitor, the number of cycles k_x needed for V_C to reach a given voltage level V_x can be derived from equation (2) under the assumption $C_b \gg C_P$ leading to

$$k_x = \frac{\ln\left(1 - \frac{V_x}{2V_{PM}}\right)}{\ln\left(\frac{C_b}{C_P + C_b}\right)} \cong \frac{C_b}{C_P} \ln\left(\frac{2V_{PM}}{2V_{PM} - V_x}\right). \qquad (3)$$

It can be seen that the period index k_x, i.e. the charging time, increases proportionally with C_b. On the other hand, for a given V_x, C_b is also linearly related to the energy stored and available for powering the load.

Therefore, for a given value of V_x as required by the proper operation of the circuitry that follows the rectifier and storage stage, the capacitor C_b must be selected as a trade-off between energy need and charging time.

If the diode voltage drops and leakage currents were considered, the term $(2V_{PM})$ in equations (1)–(3) would be reduced accordingly, but the general conclusions would be unchanged.

The energy stored in the capacitor C_b is then periodically transferred to the load through the sensing-and-switching block. This block is particularly critical, because it must have very low losses, to avoid charge leakage from the storage capacitor C_b, and provide commutations as fast as possible when the voltage V_C crosses defined high and low threshold levels. For this purpose, a tailored circuit based on discrete MOS transistors was designed, which will be described elsewhere, which provides values of the high and low threshold voltages of around 8 V and 2 V, respectively.

The voltage regulator (MAX666) generates an output voltage of 2.1 V, set by means of a resistive network, when the sensing-and-switching block is enabled. The power supply is then transferred to the sensor impedance-controlled oscillators and RF transmitter through an SPDT switch, formed by MOS transistors M_1, M_2 and M_3 (Vishay Si033 and Si035), driven by a low-power CMOS monostable circuit (TLC555). The pulse width T_M of the monostable output, which determines the duration of the frame relative to sensor 1, was set to about 3 ms, which corresponds to around one-half of the typical duration of the complete RF burst.

The sensor impedance-controlled oscillators were made by a pair of CMOS low-power astable relaxation oscillators (TLC555). As sensors 1 and 2, a variable-resistance element and a variable-capacitance element were used, denoted in figure 4 as R_S and C_S, respectively. The central values of the oscillator output frequencies f_{OSC1} and f_{OSC2} were set to about 25 and 50 kHz, with the duty cycle slightly greater than 50%, for nominal sensor values of 10 kΩ and 470 pF, respectively.

The frequency-modulated square-wave output signals of the astable oscillators are then used for the OOK modulation of the 315 MHz RF carrier of a low-power RF transmitter (MAX1472). In the performed tests, an externally powered RF receiver (MAX1473) was used to receive and demodulate the transmitted signals. The receiver bandwidth was set to about 100 kHz in order to comply with the modulation frequencies of both sensors. Figure 5(b) shows the assembled prototype of the autonomous sensor module inclusive of the piezoelectric energy converter.

4. Experimental results

Initially the frequency response of the piezoelectric converter was measured by exciting the piezoelectric converter with a sinusoidal vertical acceleration by means of an electrodynamic shaker (Bruel and Kjaer 4290). A gain-phase analyzer

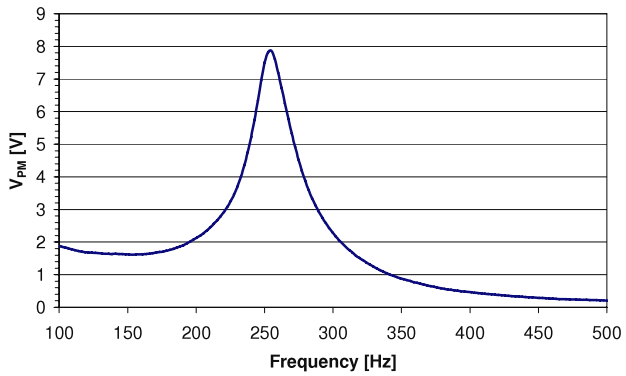

Figure 7. Measured frequency response of the piezoelectric converter.

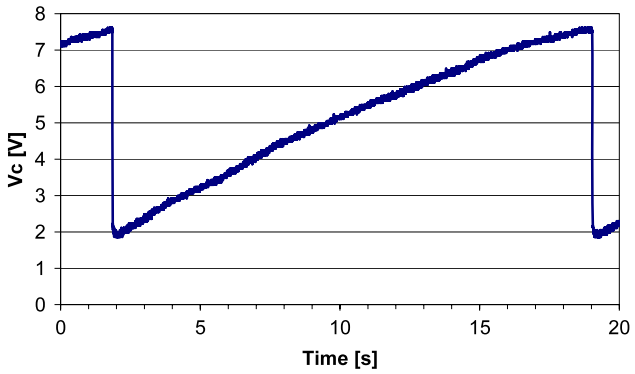

Figure 9. Typical measured voltage V_C across the storage capacitor C_b during charge–discharge cycles.

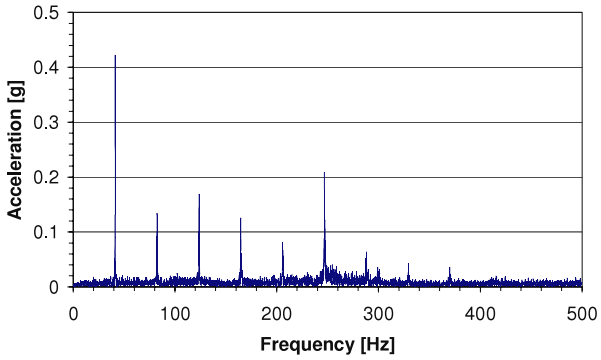

Figure 8. Measured acceleration spectrum of the mechanical excitation used in the tests.

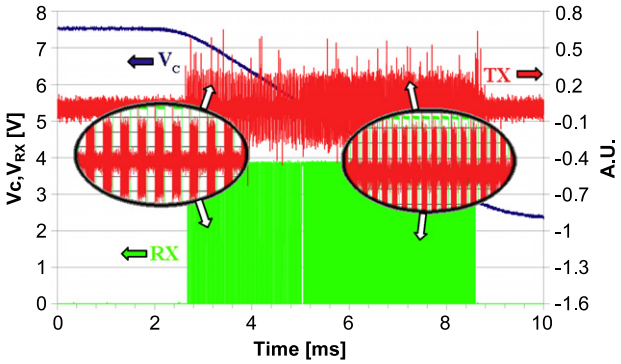

Figure 10. Typical measured voltage V_C, transmitted burst and received signal V_{RX} with enlarged views of the two frames which have the frequency respectively determined by sensor 1 and sensor 2.

(HP4194A) was used to drive the shaker and measure the open-circuit output voltage V_P generated by the piezoelectric converter in a frequency range between 100 and 500 Hz. The peak amplitude of the applied vertical acceleration was set to a constant level of $0.5g$.

Figure 7 shows the obtained frequency response peaked around the converter resonant frequency at about 250 Hz. In the tested conditions the peak output voltage V_{PM} at resonance is about 8 V. Such a value is suitable for yielding a voltage V_C of the order of volts, as discussed in section 3. The quality factor is around 10, which is a deliberately low value in order to keep the bandwidth as large as possible. It can be observed that for V_{PM} to decrease by an order of magnitude the excitation frequency has to be displaced off resonance by about 100 Hz.

The frequency dependence of the output is intrinsic for resonant converters which operate at best when most of the excitation spectrum is located within the converter bandwidth. If this condition does not apply and wideband or frequency-varying vibrations are present, a possible option is using a converter array in order to improve conversion effectiveness [19, 20].

The next tests were performed with the piezoelectric converter subject to stationary mechanical excitation by using a vibration generator realized by a DC motor with an unbalanced flywheel. The motor rotation speed was adjusted to obtain a vertical acceleration with a peak amplitude value of about $1g$. The mechanical acceleration is a periodic signal with a fundamental frequency f_{exc} of about 41 Hz. In this way the sixth harmonic of f_{exc} is located at 246 Hz, around the resonant frequency of the piezoelectric converter. In figure 8 the spectrum of the mechanical vibrations is shown, where the fundamental frequency f_{exc} and the harmonics are visible.

Under this excitation condition, the open-circuit voltage V_P of the converter is typically about 30 V peak to peak, and, with the sensor module connected, the time between two consecutive RF transmissions is about 17 s. Figure 9 reports the typical measured voltage V_C across the storage capacitor $C_b = 4.7\ \mu$F during a charging–discharging cycle. The typical intermittent operation of the system that is powered only during capacitor discharge events is visible.

In a first set of tests, in place of R_S and C_S for sensors 1 and 2, a 10 kΩ resistor and a 470 pF capacitor were used, respectively. Figure 10 shows the typical voltage V_C measured across the storage capacitor, the transmitted burst and the received signal V_{RX}, when the system is powered with the stored energy. Enlarged views of the waveforms forming the two frames relative to oscillators 1 and 2 are also shown. The transmitted burst has a total duration of about 6 ms. In the enlarged views the transmitted OOK frequency-modulated signal and the envelope of the received signal can be seen. The average power consumption during transmission was around 20 mW. The transmission range was of the order of a few meters in a laboratory environment.

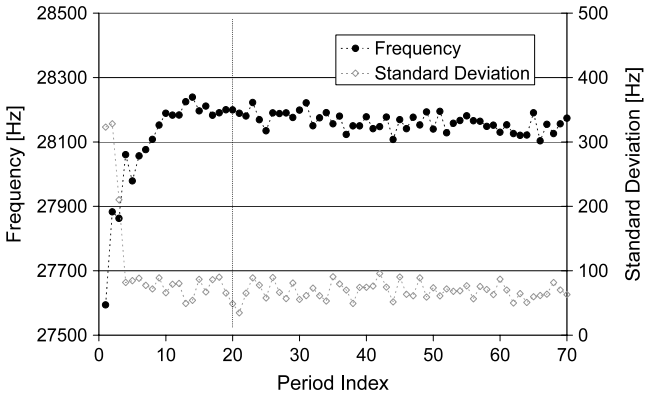

Figure 11. Measured single-period frequency versus period index along the frame averaged over 10 consecutive transmitted bursts.

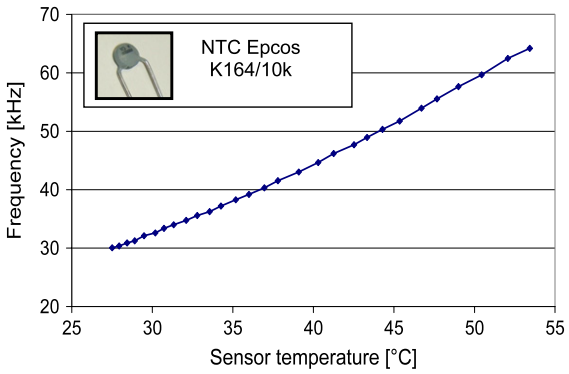

Figure 12. Frequency of the OOK modulation of the received RF signal versus sensor temperature (sensor 1).

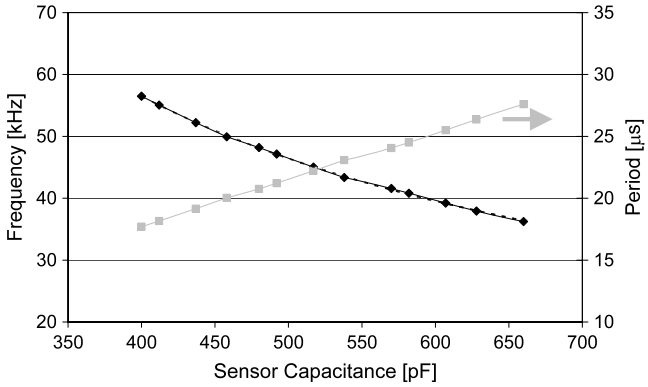

Figure 13. Frequency and period of the OOK modulation of the received RF signal versus capacitance C_S (sensor 2).

The experimental results shown in figure 10 demonstrate that the stored energy can be effectively used to generate an amount of power suitable to supply two sensor blocks and intermittently transmit their outputs.

Measurements of the frequency of the received burst were then performed with a digital counter (Philips PM6680) in order to evaluate the performance of the developed autonomous sensor module. To evaluate the stability of the frequency, measurements were performed on a single period of the received frame, and then the trend of the frequency was determined by changing the index of the considered period, i.e. by stepping the position along the frame of the period whose frequency was measured.

Figure 11 shows the measured single-period frequency of the first frame of the received burst versus the period index along the frame. Each plotted pair of frequency and standard deviation was obtained from the average of 10 repeated measurements relative to the same period index over 10 consecutive transmitted bursts. Figure 11 clearly shows an initial settling trend for the first periods in the frame, most likely due to the time required by the circuit to reach a suitable regime condition. A similar behavior was observed for the second frame. As a consequence, the first 20 periods of each of the two frames were neglected in the following tests, and the subsequent 50 adjacent periods were retained and used for the averaged measurement of the respective frequencies.

The repeatability was then tested by measuring the standard deviation σ of the frequency readings over 30 consecutive repetitions of the transmission burst, under intermittent operation mode, without changing the values of the test resistor R_S and capacitor C_S. A value of σ of less than 10 Hz resulted.

Afterward, a resistive temperature sensor (NTC thermistor Epcos K164/10k) and a variable capacitor were inserted respectively as sensor 1 (R_S) and sensor 2 (C_S). The resulting frequency f_{OSC1} was about 30 kHz at 27.5 °C, and the frequency f_{OSC2} was about 50 kHz for $C_S = 470$ pF. The system was tested under the excitation conditions described in figure 8, in order to work in an intermittent operation mode, while applying different temperature values to the thermistor by means of a resistive heater, and varying C_S across different capacitance values. This conditions exemplify the possible application of a sensor module mounted on a machinery part for thermal condition monitoring purposes.

Figures 12 and 13 show the frequencies measured at the output of the RF receiver for the same transmission burst respectively versus temperature (signal from sensor 1 measured in the first frame of the burst), and versus capacitance C_S (signal from sensor 2 measured in the second frame of the burst).

In figure 12, a frequency variation across a wide range can be observed with, incidentally, a fairly good linearity that depends on the combination of the thermistor characteristic curve and the resistance-to-frequency conversion function of the relaxation oscillator, as described in figure 4. An average sensitivity of about 1.3 kHz $°C^{-1}$ results over the explored temperature range between 27 and 54 °C. Considering the above-quoted frequency standard deviation $\sigma = 10$ Hz, the nominal temperature resolution, calculated at 3σ, for a single burst reading is about 0.02 °C.

Figure 13 shows both the frequency and the period measured at the output of the RF receiver versus the capacitance C_S. The behavior of the period is linear according to the capacitance-to-period conversion function of the oscillator of figure 4, while the behavior of the frequency, despite the hyperbolic capacitance-to-frequency relationship, also presents a fairly good linearity due to the narrow range of the capacitance values tested. From the average sensitivity of

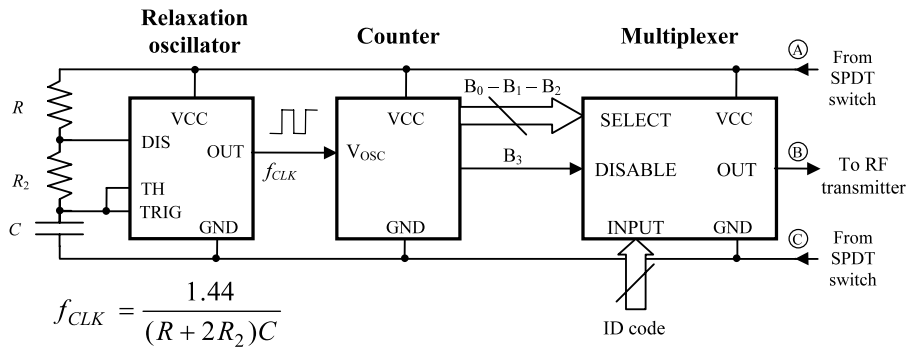

Figure 14. ID code generation circuit.

about -80 Hz pF^{-1}, and considering the measured frequency standard deviation $\sigma = 10$ Hz, the resulting nominal resolution calculated at 3σ is about 0.4 pF.

As an additional development, the architecture proposed and shown in figure 3 was breadboarded and tested. In this case, the system of figure 4 was modified by replacing sensor 2 and the respective circuit block by an 8-bit ID code generation circuit. Therefore, the first transmitted frame of the RF burst carries the reading of the sensor, while the second frame contains the ID code as a tag of the transmitting sensor unit.

As shown in figure 14, the ID code generation circuit is formed by a fixed-frequency relaxation oscillator (TLC555), a 4-bit binary counter (SN74HC393) and a 8-to-1 digital multiplexer (SN74HC151). The relaxation oscillator works as a clock generator with a frequency $f_{\mathrm{CLK}} = 82$ kHz.

The three less significant bits of the counter B_0, B_1 and B_2 are used to cyclically select the 8 inputs of the multiplexer (MUX), that are set to the desired 8-bit ID code, while the most significant bit B_3 is used to disable the output of the MUX. In this way the ID code is cyclically serialized with an idle time of eight clock periods between two consecutive code transmissions. The insertion of a fixed time interval between two serializations allows a simple timing and synchronization at the receiver to extract the ID code.

The autonomous sensor system was tested in the same excitation conditions as described previously. The piezoelectric converter excited by using a vibration generator was used to power the system. The peak of the vertical acceleration was about $1g$ at a frequency of about 41 Hz. With a storage capacitor C_b of 6.9 μF, the time between two consecutive transmissions was about 25 s while the transmission time was 12 ms. The pulse width T_{M} of the monostable output was set to be about 5 ms.

Figure 15 shows the typical voltage V_C measured across the storage capacitor, the transmitted burst and the received signal V_{RX}, with enlarged views of the waveforms relative to the two frames. In the second frame the cyclic repetition of the ID code transmission can be seen, which in this case was set to 10101111.

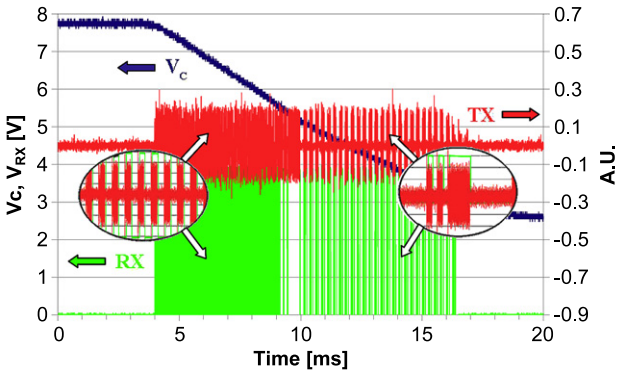

Figure 15. Typical measured voltage V_C, transmitted burst and received signal V_{RX} with enlarged views of the two frames which represent respectively the frequency determined by sensor 1 and the system ID code.

5. Conclusions

An autonomous sensor module powered by a piezoelectric energy converter from background vibrations is presented. The module interfaces to two passive sensors, and intermittently transmits their measurement signals by frequency-modulating, via OOK coding, the envelope of an RF carrier burst. The method can be generalized to more than two sensors and offers the advantage that the measurement signals are sent in analog form on the timescale, avoiding the use of on-board ADCs which would set the resolution limit *a priori*. As an additional variant, the module can send a programmable 8-bit identification (ID) code on the signal RF carrier in order to enable module tagging and tracking by the external receiver unit.

The architecture and principle have been experimentally validated on fabricated prototypes including a commercial piezoelectric bimorph converter and a resistive–capacitive sensor pair made by a thermistor plus a variable capacitor. The electronic circuitry was assembled using purposely chosen low-power off-the-shelf components.

In the tested experimental conditions, the typical time interval between measurement-and-transmission events was of the order of a few tens of seconds, with event durations of the order of a few tens of milliseconds. This corresponds to an operation duty-cycle of the order of 0.1%.

The conditions to best retrieve the sensor measurement values from the frequencies measured at the external RF receiver were investigated. It was found that, provided we allow for a limited number of signal periods to settle

the frequency at the beginning of each transmitted frame, a repeatability of the order of a few hundred ppm of the transmitted sensor frequency was achievable over 30 repetitions. This, combined with the sensor sensitivity, can determine considerable values of measurement resolution.

The obtained results show that the proposed approach has attractive characteristics because of the total absence of batteries and, despite the inherent intermittent operation and the related design challenges, ensures significant measurement performance.

It is expected that, by improving the energy converter stage, for example using a multi-frequency converter array (MFCA) [20] and reducing the power consumption of the electronics by an optimized design [21], the operation duty cycle can be increased substantially at parity of mechanical excitation, without decreasing the measurement performance.

Acknowledgment

The work was partially carried out under project PRIN2007-20078ZCC92 co-funded by the Italian MIUR.

References

[1] Cook-Chennault K A, Thambi N and Sastry A M 2008 Powering MEMS portable devices—a review of non-regenerative and regenerative power supply systems with special emphasis on piezoelectric energy harvesting systems *Smart Mater. Struct.* **17** 1–33

[2] Gonzàlez J L, Rubio A and Moll F 2002 Human powered piezoelectric batteries to supply power to wearable electronic devices *Int. J. Soc. Mater. Eng. Resour.* **10** 33–40

[3] Kymissis J, Kendall C J, Paradiso J and Gershenfeld N 1998 Parasitic power harvesting in shoes *ISWC: Proc. 2nd IEEE Int. Conf. on Wearable Computing (Pittsburgh, PA, Oct. 1998)* pp 132–9

[4] Starner T 1996 Human-powered wearable computing *IBM Syst. J.* **35** 618–29

[5] Mathúna C Ó, O'Donnell T, Martinez-Catala R V, Rohan J and O'Flynn B 2008 Energy scavenging for long-term deployable wireless sensor networks *Talanta* **75** 613–23

[6] Mitcheson P D, Yeatman E M, Rao G K, Holmes A S and Green T C 2008 Energy harvesting from human and machine motion for wireless electronic devices *Proc. IEEE* **96** 1454–86

[7] Roundy S, Wright P K and Rabaey J 2003 A study of low level vibrations as a power source for wireless sensor nodes *Comput. Commun.* **26** 1131–44

[8] Sterken T, Baert K, Van Hoof C, Puers R, Borghs G and Fiorini P 2004 Comparative modelling for vibration scavengers *Proc. IEEE Sensors 2004 (Vienna, Oct. 2004)* vol 3, pp 1249–52

[9] James E P, Tudor M J, Beeby S P, Harris N R, Glynne-Jones P, Ross J N and White N M 2004 An investigation of self-powered systems for condition monitoring applications *Sensors Actuators* A **110** 171–6

[10] Roundy S and Wright P K 2004 A piezoelectric vibration based generator for wireless electronics *Smart Mater. Struct.* **13** 1131–42

[11] Umeda M, Nakamura K and Ueha S 1997 Energy storage characteristics of a piezogenerator using impact vibration *Japan. J. Appl. Phys.* **36** 3146–51

[12] Ottman G K, Hofmann H, Bhatt A C and Lesieutre G A 2002 Adaptive piezoelectric energy harvesting circuit for wireless, remote power supply *IEEE Trans. Power Electron.* **17** 669–76

[13] Beeby S P, Tudor M J and White N M 2006 Energy harvesting vibration sources for microsystems applications *Meas. Sci. Technol.* **17** 175–95

[14] Mitcheson P D, Green T C and Yeatman E M 2007 Power processing circuits for electromagnetic, electrostatic and piezoelectric inertial energy scavengers *Microsyst. Technol.* **13** 1629–35

[15] Lefeuvre E, Badel A, Richard C, Petit L and Guyomar D 2006 A comparison between several vibration-powered piezoelectric generators for standalone systems *Sensors Actuators* A **126** 405–16

[16] Ferrari M, Ferrari V, Marioli D and Taroni A 2006 Modeling, fabrication and performance measurements of a piezoelectric energy converter for power harvesting in autonomous microsystems *IEEE Trans. Instrum. Meas.* **55** 2096–101

[17] Ferrari M, Ferrari V, Marioli D and Taroni A 2005 Thick-film piezoelectric energy converter for power harvesting in autonomous microsystems *Proc. Eurosensors XIX Conf. (Barcelona, Sept. 2005)*

[18] Renaud M, Karakaya K, Sterken T, Fiorini P, Van Hoof C and Puers R 2008 Fabrication, modelling and characterization of MEMS piezoelectric vibration harvesters *Sensors Actuators* A **145/146** 380–6

[19] Liu J-Q, Fang H-B, Xu Z-Y, Mao X-H, Shen X-C, Chen D, Liao H and Cai B-C 2008 A MEMS-based piezoelectric power generator array for vibration energy harvesting *Microelectron. J.* **39** 802–6

[20] Ferrari M, Ferrari V, Guizzetti M, Marioli D and Taroni A 2008 Piezoelectric multifrequency energy converter for power harvesting in autonomous microsystems *Sensors Actuators* A **142** 329–35

[21] Colomer-Farrarons J, Miribel-Català P, Saiz-Vela A, Puig-Vidal M and Samitier J 2008 Power-conditioning circuitry for a self-powered system based on micro PZT generators in a 0.13 μm low-voltage low-power technology *IEEE Trans. Indust. Electron.* **55** 3249–57